

34. In a series of experiments, the Harvard group inverted synthetic data sets calculated for shear-velocity structures specified by a single spherical-harmonic Chebyshev coefficient,  $\beta^n$ . Figure 2D compares the radial correlation lengths computed from the input structures with the values for the recovered models for two examples,  $\beta_{10}^5$  and  $\beta_{11}^6$ . In the first case, the inversion faithfully reproduces the  $n = 5$  checkerboard pattern of  $R_\beta(r, r')$  and the sawtooth variation of  $\rho_{0.75}(r)$  to depths on the order of 2000 km. The second shows more degradation in the lowermost mantle as well as some loss of detail in the uppermost mantle, but even at these higher wave numbers ( $n = 8, l = 11$ ) the correlation-length minimum near 670 km is reproduced with only a minor loss of amplitude.
35. The difference in the radial correlation functions for the two seismic models becomes large in the lowermost mantle (Fig. 2C), where the current data sets have poor resolving power (34). In the Harvard model,  $\rho_{0.75}(r)$  begins to increase at a depth of 1500 km and reaches a maximum of 320 km at 2400 km, the depth that marks the best expression of the dominant high-amplitude, low-degree structures. In the Scripps model, these features are compressed into a thinner zone above the core-mantle boundary;  $\rho_{0.75}$  remains approximately constant down to 2400 km, increasing to 270 km at the base of the mantle. These differing structures, which fit the data about the same, exemplify the nonuniqueness associated with the trade-off between radial and angular smoothness (G. Masters, personal communication, 1993).
36. Tanimoto (20) computed layer correlation coefficients for the degree-two components of his whole-mantle model MDLSH (9) and noted a low or negative correlation between layers above and below 1000-km depth, which he took as evidence for stratification. Individual spherical-harmonic components of whole-mantle convection simulations typically show strong, time-dependent radial decorrelations not evident in the heterogeneity fields expanded to  $l_{\max} \geq 6$ . There is no evidence for a correlation-length minimum in Tanimoto's complete degree-six model.
37. We also examined two degree-eight tomographic models from an earlier Harvard study (11). The first, SH8/WMM13, has the same radial parameterization as SH12/WMM13 ( $n = 13$ ), and its radial correlation function is similar to the one displayed in the top panel of Fig. 4. The second, SH8/U4L8, is parameterized by separate Chebyshev expansions in the upper mantle ( $n = 4$ ) and lower mantle ( $n = 8$ ) and therefore develops a discontinuity in  $\delta\beta$  at a depth of 670 km. This model displays a sharp decrease in  $\rho_{0.75}(r)$  confined to a 200-km interval centered on the 670-km discontinuity. This feature is much smaller in amplitude and radial scale than the decorrelation signatures associated with the stratified convection models discussed in the text and is probably an artifact of the discontinuous parameterization. A tomographic model can be represented as the output of a filter whose input is the real Earth and whose response is determined by the seismic data and the model parameterization. The transition-zone variation observed in the  $\rho_{0.75}(r)$  values for SH8/U4L8 is reproduced almost exactly by the passing of an Earth structure having a smooth radial correlation function through the SH8/U4L8 parameterization filter. This calculation suggests that discontinuous model parameterizations should be avoided in tomographic tests of mantle stratification.
38. T. H. Jordan and W. S. Lynn, *J. Geophys. Res.* **79**, 2679 (1974); T. H. Jordan, *J. Geophys. Res.* **43**, 473 (1977); S. P. Grand, *J. Geophys. Res.* **92**, 14065 (1987); K. M. Fischer, K. C. Creager, T. H. Jordan, *ibid.*, **96**, 14403 (1991).
39. D. Giardini and J. H. Woodhouse, *Nature* **307**, 505 (1984); K. M. Fischer and T. H. Jordan, *J. Geophys. Res.* **96**, 14429 (1991); R. van der Hilst, E. R. Engdahl, W. Spakman, G. Nolet, *Nature* **353**, 37 (1991); Y. Fukao, M. Obayashi, H. Inoue, M. Nenbai, *J. Geophys. Res.* **97**, 4809 (1992); P. M.

Shearer and T. G. Masters, *Nature* **355**, 791 (1992).

40. We thank A. Dziewonski, W.-J. Su, and R. Woodward for their unpublished Earth models and resolution analysis; G. Masters, H. Bolton, and P. Shearer for their unpublished Earth model; and B.

Hager for helpful discussions. Supported by grants from the U.S. National Science Foundation and by the Institute of Geophysics and Planetary Physics at Los Alamos National Laboratory.

6 May 1993; accepted 8 July 1993

## Late Cretaceous Precessional Cycles in Double Time: A Warm-Earth Milankovitch Response

J. Park, S. L. D'Hondt, J. W. King, C. Gibson

Late Cretaceous climatic cycles are reflected in lithological and magnetic variations in carbonate sediments from South Atlantic Deep-Sea Drilling Project site 516F at a paleo-latitude of roughly 30°S. Magnetic susceptibility cycles 20 to 60 centimeters in length appear to be controlled by the precession of the equinoxes. Cyclicity is particularly robust within a 24-meter interval in the lower Campanian, where overtone spectral peaks are observed as well as secondary susceptibility maxima within individual precession cycles. One model for this behavior is that sedimentation in the narrow Cretaceous South Atlantic was controlled by equatorial climate dynamics, with the precessional insolation signal rectified by the large land masses surrounding the ocean basin.

Quasi-periodic oscillations in the Earth's orbit about the sun cause variations in the amount and distribution of insolation received at the Earth's surface. In the last million years, the Milankovitch orbital cycles of precession, obliquity, and eccentricity are thought to have governed the Earth's climate (1). Orbital cycles exerted a strong influence on the climate of the Earth during the Cretaceous, as evidenced by cyclic variations in Cretaceous deep-sea and shelf sedimentary rocks (2). Because the fluctuations associated with orbital cycles are at most 10% of the mean insolation, the Earth's climate may often have been quite sensitive to externally determined conditions. As a consequence, the geologic record of orbital cycles shows how the Earth's climate responds to modest perturbations and may help us to anticipate future anthropogenic climate trends.

Mesozoic sedimentary records are often marred by large variations in accumulation rate and diagenesis (3). Fourier analysis of Mesozoic climate proxy data typically offers only a rough estimate of the data's spectral properties. Data of much higher quality can be found in drill cores from Deep-Sea Drilling Project (DSDP) site 516F, on the Rio Grande Rise in the South Atlantic Ocean. In one interval of these data, the accumulation rate appears nearly constant for roughly 1 million years, so that fine details of the climate proxy spectrum can be estimated. These details shed light on the

climate dynamics of the warm Cretaceous.

The Cretaceous-Paleocene part of the site 516F data consists largely of alternating carbonate and marl layers of varying color, deposited at bathyal depths (500 to 1500 m) (4). In an earlier orbital-cycle analysis of this and other South Atlantic sites, optical densitometry was used to estimate an average duration of  $23.5 \pm 4.4 \times 10^3$  years for the Cretaceous lithologic cycles (5), close to the principal modern precessional periods of  $19.0 \times 10^3$ ,  $22.4 \times 10^3$ , and  $23.7 \times 10^3$  years. We have measured whole-core magnetic susceptibility from core segments spanning the Santonian [ $\sim 85$  Ma (million years ago)] through the earliest Danian ( $\sim 64$  Ma). Magnetic susceptibility in carbonate sediments is influenced by many factors but is typically dominated by the ratio of terrigenous to biogenic components (6, 7). Chalky layers typically have lower susceptibility than marly layers. Depending on the sedimentary environment, cyclic variations in susceptibility can be governed by terrigenous input, carbonate dissolution, or dilution by biogenic carbonate production.

Distinct cyclostratigraphic patterns appear to persist for a few tens of meters within the site 516F record, corresponding to intervals of a few million years. Cores 113, 114, and 115 are part of one such stable interval, lying within the lower Campanian (8) (Fig. 1). Short cycles are grouped into bundles of four or five, consistent with the modulation of precessional insolation variations by the Earth's orbital eccentricity. Drilling records (4) indicate that little material was lost between the core segments; core 115 is truncated, but the sum of cores 112, 113, and 114 differs by only 1 cm from nominal perfect

J. Park, Department of Geology and Geophysics, Post Office Box 6666, Yale University, New Haven, CT 06511.

S. L. D'Hondt, J. W. King, C. Gibson, Graduate School of Oceanography, University of Rhode Island, Narragansett, RI 02882.

recovery. We therefore combined the records sequentially for spectral analysis. The adaptive multitaper spectral estimate (9) of this data series (Fig. 2) shows three spectral peaks at roughly 1.9, 2.35, and 2.9 cycles per meter. The ratios of the wavelengths corresponding to these frequencies approximate those of the major precession periods of  $22.4$  to  $23.7 \times 10^3$ ,  $19.0 \times 10^3$ , and  $16.9 \times 10^3$  years. Scaling by the putative  $19.0 \times 10^3$  year peak, we estimate that the accumulation rate was  $22.4$  m per million years. The estimated duration of the data series is roughly  $1.1 \times 10^6$  years, not long enough to separate the  $22.4 \times 10^3$  and  $23.7 \times 10^3$  year cycles, which appear as a single spectral peak. Little spectral energy is evident in the susceptibility data at wavelengths corresponding to the obliquity cycle. This observation suggests that high-latitude climate influences the record weakly if at all. The broad spectral maximum at wavelengths corresponding to the eccentricity periods near  $100 \times 10^3$  years reflects the "bundling" of precession cycles in the time domain. Eccentricity does not generate a  $100 \times 10^3$  year peak in the insolation spectrum, but its modulation of precession, coupled with a nonlinear Earth-system response, can lead to eccentricity peaks in climate proxy spectra (9-11).

Several peaks in the susceptibility spectrum estimate are evident at frequencies higher than those identified with precession. Examination of the  $F$  variance-ratio test for phase-coherent sinusoids (9) reveals, at better than 95% confidence for nonrandomness, periodic spectral lines at the sums  $f_1 + f_2$ ,  $2f_1$ , and  $2f_2$  of the frequencies  $f_1$  and  $f_2$  of the largest spectral peaks, which we identify with the  $22.4$  to  $23.7 \times 10^3$  year and  $19.0 \times 10^3$  year precession periods. Second overtones, as well as first overtones, can be observed in spectral estimates from individual cores 113 and 115 and are statistically correlated with the fundamental peak (Fig. 3). Overtone spectral peaks occur when a system re-

sponds nonlinearly to a periodic input forcing. Close examination of the site 516F data series (Fig. 4) reveals that the precession cycle often exhibits secondary susceptibility maxima. Similar behavior is found in susceptibility data from site 516F cores 112 through 116. Spectra from cores 112 and 116 show only broad peaks, however, due to changes in cycle thickness that are visible in the data. We interpret this weak double beat as evidence that the sedimentary environment in the Brazil Basin in this interval responded in a similar manner to the opposite extremes of the precessional insolation cycle. Roughly 41 m of sediment at site 516F show this behavior (this is a lower bound due to coring gaps), corresponding to nearly  $2 \times 10^6$  years.

Fine-scale limestone-marl and black shale layering has been described in drill cores from the Cretaceous South Atlantic by many researchers (4, 5, 12-14). In the Cretaceous the South Atlantic was much narrower than at present. In simulations of Cretaceous climate with atmospheric global circulation models (GCMs) (15), the restriction of this source of moisture between Africa and South America tends to fix the location of evaporative maxima in the equatorial Intertropical Convergence Zone (ITCZ). Superimposed on this pattern, precessional insolation variations modulate the strength of the monsoonal pressure extrema over the southern continents. In the GCM simulations, associated changes in monsoonal wind patterns cause cyclic shifts in the evaporation minus precipitation balance over the equatorial South Atlantic.

Deep-water circulation in the Santonian and early Campanian Brazil and Angola basins was likely isolated from the world ocean; water exchange was primarily over sills at the Rio Grande Rise and the Walvis Ridge (16). Park and Oglesby (15) argued that the evaporation minus precipitation shifts seen in the GCM simulations would

lead to an alternation between lagoonal and estuarine circulation in the low-latitude South Atlantic. The scenario, and its geochemical consequences, has been proposed to explain cyclic anoxia in Plio-Pleistocene sediments in the Mediterranean (17, 18) and may contribute to the lithologic variations seen throughout the Cretaceous interval of South Atlantic drill cores. Excess precipitation over a restricted basin leads to an exchange of less saline surface waters for oxygen-poor, nutrient-rich intermediate waters from the larger ocean (estuarine circulation); enhanced biological productivity and the reduced nutrients consume the remaining oxygen, and anoxia develops (18). If evaporation dominates over a restricted basin, the basin draws surface waters from the larger ocean and exports saline, nutrient-poor, deep, or intermediate water (lagoonal circulation). An increase in magnetic susceptibility can be generated in this model by decreased carbonate production, increased carbonate dissolution, or increased riverine input during periods of net precipitation. Alternatively, increased eolian influx could result in susceptibility maxima during intervals of net evaporation.

Although the above scenario suggests why

**Fig. 1.** Whole-core magnetic susceptibility (in scaled units) for cores 113, 114, and 115 of DSDP site 516F, logged at 3-cm intervals with a Bartington Instruments MS-2 system with loop sensor. The interval was drilled between 1145.1 and 1169.0 m beneath the sea floor. The Santonian-Campanian boundary was inferred to lie at 1161 m, but other data suggest it is deeper, at least 1200 m (8). The lithology is primarily intercalated gray limestone and dark greenish gray marly limestone. Bioturbation is evident but does not appear to affect variations with a scale length of  $\geq 10$  cm.

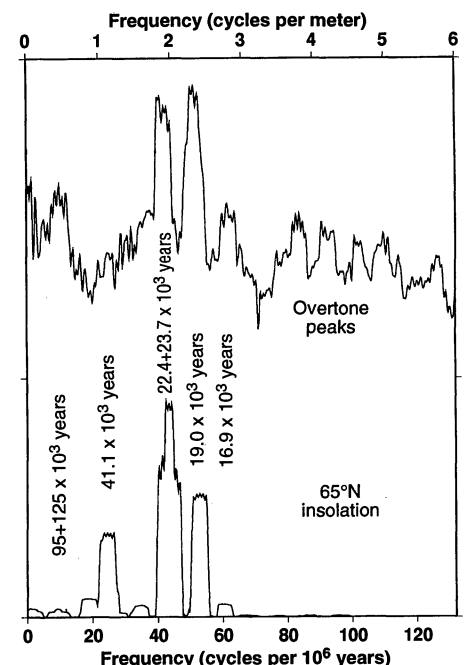
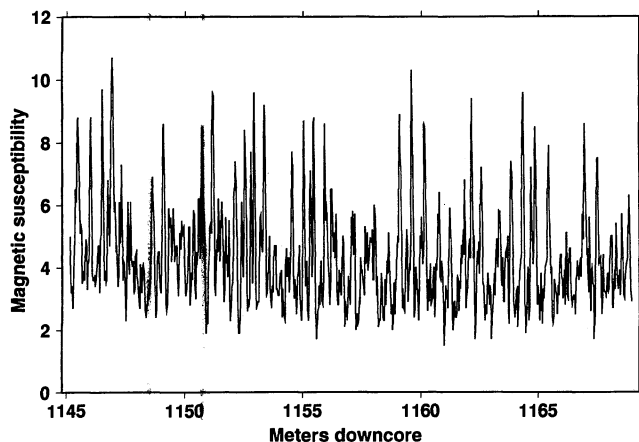


**Fig. 2.** The adaptive multitaper spectrum estimate (9) of the site 516F magnetic susceptibility data series based on the use of five  $3\pi$ -prolate Slepian tapers. The amplitude spectrum is plotted at the top. For white processes, this estimator follows a  $\chi^2$  distribution with 10 degrees of freedom and averages spectral information over a bandwidth  $\Delta f = 0.25$  cycle per meter. The spectrum estimate of a  $1.1 \times 10^6$  year astronomical series of Pleistocene insolation (10) at  $65^\circ\text{N}$  is shown at the bottom for comparison.

precession should modulate South Atlantic lithologic cycles, it does not explain the observed double beat. Two possible explanations are (i) sensitivity of South Atlantic circulation to two separate high-latitude sources of deep water, north and south of the equator and (ii) nonlinear response to orbital forcing in an equatorial region. The position of site 516F in southern mid-latitudes and the lack of a Santonian or early Campanian deep-water connection between the Brazil Basin and high latitudes make the first explanation unlikely. The second explanation is supported by a recent modeling study by Short *et al.* (11), which simulated the yearly temperature cycle in the Plio-Pleistocene with a linear energy-balance model. In this study, climate response was quantified by  $T_{\max}$ , the maximum yearly surface temperature. A double-beat response to precession was found at equatorial locations on or proximal to large land masses. Temperature over continents that straddle the equator is sensitive to both extremes of the preces-

sion cycle, as a part of the land mass will receive maximum insolation at each solstice. Monsoonal wind patterns strengthen and diminish with air pressure anomalies developed over regions of continental heating, so an equatorial  $T_{\max}$  signal would be transported poleward, its reach limited by the extent of monsoonal circulation. The nonlinearity in this scenario arises from the assumption that the sedimentary system is linked to the maximum yearly temperature in the continental interior, which does not depend linearly on the integrated insolation on the land mass. Short *et al.* suggested that their model response may explain 10 to  $12 \times 10^3$  year variations in Quaternary Saharan aridity (19).

The time series record of simulated  $T_{\max}$  for a test point in Pleistocene equatorial Africa (11) is remarkably similar to the magnetic susceptibility record for the lower Campanian interval from DSDP site 516F. The sediments at site 516F, however, were deposited at a paleolatitude of  $\geq 30^\circ\text{S}$ , sug-

gesting that the effect of climate variability at the equator was felt in mid-latitudes. Broad low-pressure systems may have developed over the combined African–South American land mass as a result of enhanced equatorial heating at the precessional extremes. As long as the South Atlantic and associated seaways were restricted in area and were warm, the larger heat capacity of the ocean might not impede the development of a single monsoonal low. The circulation around such a monsoonal low could easily extend to  $30^\circ\text{S}$ .

Sedimentological data are consistent with an equatorial monsoon scenario. Organic matter is relatively abundant, and kaolinite is the dominant clay component in the interval we analyzed. This pattern suggests that sediments deposited in this double-beat interval were derived from a relatively warm, humid, and equable paleoenvironment (20, 21). Surprisingly, kaolinite was not deposited at DSDP site 357, which is farther from the Rio Grande Rise and in deeper water. This suggests that the kaolinite source was localized on a subaerial part of the rise (21).

To an extent, the equatorial monsoon hypothesis is consistent with GCM experiments (15) that suggest that low-latitude monsoonal cycles influence the circulation of the Cretaceous Brazil and Angola basins. However, most GCM simulations for the Cretaceous have used drastically simplified boundary conditions and assumptions of an ice-free Earth with uniform land conditions, usually grassland or bare soil. GCM simulations suggest (22) that climate changes associated directly with the widening South Atlantic are small in comparison to changes associated with variations in sea-surface temperature. A likely necessary condition for the formation of a large equatorial low-pressure anomaly over the combined Africa and South America was the thermal isolation of the Brazil and Angola basins, but this has not been investigated. Either thermal subsidence of the Rio Grande Rise and Falkland Plateau (23) or opening of the South Atlantic to greater exchange with the North Atlantic (16) eventually allowed cooler high-latitude waters into this region. This would weaken an African–South American monsoon and strengthen meridional (north-south) temperature gradients. This monsoonal model is testable by further numerical climate studies and by sedimentologic analyses of other Late Cretaceous marine sequences. We expect the double beat to be present in coeval South Atlantic sequences but absent from sediments deposited in cooler intervals. Within the context of site 516F, the latter prediction is satisfied, as this double-beat interval is succeeded by different cyclostratigraphic (24) and lithologic (4) regimes in younger sediments.

**Fig. 3.** Spectral analysis of magnetic susceptibility data from site 516F core 115 (5.9 m). The adaptive multitaper spectrum estimate is shown at the margins of the plot. The gray-shade plot displays the correlation estimator  $|C(f_1, f_2)|^2$ , where

$$C(f_1, f_2) = \frac{\sum_{k=0}^{K-1} Y_k^*(f_1) Y_k(f_2)}{\left( \sum_{m=0}^{K-1} |Y_m(f_1)|^2 \sum_{j=0}^{K-1} |Y_j(f_2)|^2 \right)^{1/2}}$$

The  $k$ th eigenspectrum estimate of the susceptibility data series,  $Y_k(f)$ , is obtained by a discrete

Fourier transform of the data multiplied by the  $k$ th  $3\pi$ -prolate Slepian data taper. In this example, there are  $K = 5$  tapers, so that the 99% confidence level for nonrandomness is  $|C(f_1, f_2)|^2 \approx 0.6$ . The 19.0 and 22.4, 23.7 spectral peaks in Fig. 2 cannot be resolved with this short record length and are melded into the spectral peak at 1.8 cycles per meter. Note the strong correlation between this spectral peak and its two overtone peaks.

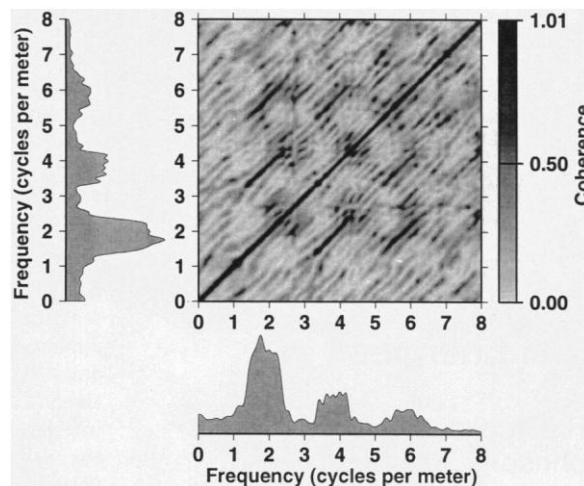
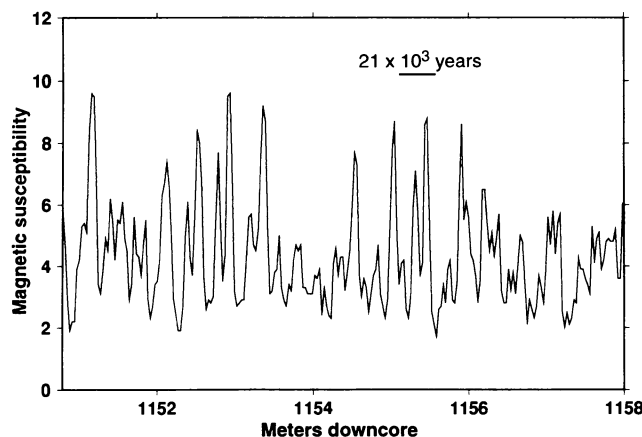


**Fig. 4.** Expanded view of the susceptibility record from DSDP site 516F, showing a portion that straddles the transition between cores 113 and 114 (at 1154.6 m). The distance (47 cm) that we interpret as the duration of an average precession cycle is shown. Note the secondary susceptibility maxima within individual cycles.



## REFERENCES AND NOTES

- J. D. Hays, J. Imbrie, N. J. Shackleton, *Science* **194**, 1121 (1976); A. Berger, *Rev. Geophys.* **26**, 624 (1988).
- E. J. Barron, M. A. Arthur, E. G. Kauffman, *Earth Planet. Sci. Lett.* **72**, 327 (1985).
- J. Park and T. D. Herbert, *J. Geophys. Res.* **92**, 14027 (1987); W. Ricken, *Diagenetic Bedding: A Model for Marl-Limestone Alternations* (Springer-Verlag, Berlin, 1986).
- P. F. Barker, R. L. Carlson, D. A. Johnson *et al.*, *Init. Rep. Deep Sea Drill. Proj.* **72**, 155 (1983).
- T. D. Herbert and S. L. D'Hondt, *Earth Planet. Sci. Lett.* **99**, 263 (1990).
- G. A. Mead, L. Tauxe, J. L. LaBrecque, *Paleoceanography* **1**, 273 (1986).
- J. Bloemendal, B. Lamb, J. King, *ibid.* **3**, 61 (1988).
- The Santonian-Campanian stage boundary was placed in core 114 of site 516F, on the basis of the first occurrence of *Globotruncana arca*, and is underlain by a 15-m unzoned region [W. Weiss, *Init. Rep. Deep Sea Drill. Proj.* **72**, 715 (1983)]. However, this places the site 516F stage boundary within the 33R magnetic chron (see N. Hamilton and A. E. Suzymov, *ibid.*, p. 723). Other researchers [for example, W. Alvarez *et al.*, *Geol. Soc. Am. Bull.* **88**, 383 (1977); S. C. Cande and D. V. Kent, *J. Geophys. Res.* **97**, 13917 (1992)] place the Santonian-Campanian stage boundary within the older 34N chron, which implies that the interval we have analyzed lay entirely within the lower Campanian.
- D. J. Thomson, *Philos. Trans. R. Soc. London* **330**, 601 (1990).
- A. Berger and M. F. Loutre, *Quat. Sci. Rev.* **10**, 297 (1991); \_\_\_\_\_, J. Laskar, *Science* **255**, 560 (1992).
- D. A. Short, J. G. Mengel, T. J. Crowley, W. T. Hyde, G. R. North, *Quat. Res.* **35**, 157 (1991).
- M. Melguen, *Init. Rep. Deep Sea Drill. Proj.* **40**, 981 (1978).
- P. E. Borella, *ibid.* **74**, 645 (1984).
- D. A. V. Stow and W. E. Dean, *ibid.* **75**, 809 (1984).
- J. Park and R. J. Oglesby, *Palaeogeogr., Palaeoclimatol. Palaeoecol.* (Global and Planetary Change Section), **90**, 329 (1991).
- F. W. McCoy and H. B. Zimmerman, *Init. Rep. Deep Sea Drill. Proj.* **39**, 1047 (1977).
- M. Rossignol-Strick, *Paleoceanography* **2**, 333 (1987).
- J. L. Sarmiento, T. D. Herbert, J. R. Toggweiler, *Global Biogeochem. Cycles* **2**, 427 (1988). This simplified box model investigates the formation of anoxic bottom water, not the oxygen-minimum zone at a depth of ~500 m inferred for organic deposits in the Cretaceous South Atlantic (20). The model of Sarmiento *et al.* is consistent with an oxygen-minimum zone if intermediate water at the sill continuously replenishes the bottom water in a stratified Brazil Basin.
- E. M. Pokras and A. C. Mix, *Nature* **326**, 486 (1987).
- W. T. Coulbourn, *Init. Rep. Deep Sea Drill. Proj.* **72**, 995 (1983).
- H. B. Zimmerman, *ibid.*, p. 383.
- J. Park and R. J. Oglesby, in *Orbital Forcing and Cyclic Sequences*, P. L. de Boer, Ed. (Blackwell, Oxford, in press).
- P. E. Barker, *Init. Rep. Deep Sea Drill. Proj.* **72**, 953 (1983).
- S. L. D'Hondt, J. W. King, C. Gibson, J. Park, *Am. Geophys. Union 1992 Fall Meeting Suppl.* **73**, 271 (1992).
- T. D. Herbert pointed out the stratigraphic inconsistency described in (8). The Ocean Drilling Project provided access to drill cores from site 516F. S.L.D'H., J.W.K., and C.G. were supported by the Marine Geology and Geophysics program of the National Science Foundation under grant OCE-9012314. J.P. was supported by NSF Presidential Young Investigator award EAR-8657206.

26 March 1993; accepted 8 July 1993

## Probing Chemical Reactions: Evidence for Exploration of an Excited Potential Energy Surface at Thermal Energies

Michael D. Barnes,\* Philip R. Brooks,† R. F. Curl,†  
Bruce R. Johnson

The reaction  $K + NaBr \rightarrow KBr + Na$  is probed during the reactive collision by a continuous wave laser tuned to frequencies not resonant with excitation in either reagents or products. Transient  $[K \cdot Br \cdot Na]$  absorbs a laser photon giving  $[K \cdot Br \cdot Na]^*$ , which can decompose to  $Na^* + KBr$ . Emission from excited  $Na^*$  at the sodium *D* lines provides direct evidence of laser absorption during the reaction. Different excitation spectra were observed, depending on which sodium *D* line was monitored. This difference is explicable if, in the absence of the laser, the reaction flux partially bifurcates to a second potential energy surface during the reaction.

Over the last few years we, among others (1), have developed methods that permit the spectroscopic probing of simple systems during chemical reaction. We report here evidence that suggests that during the reaction,  $K + NaBr \rightarrow KBr + Na$ , the system

can hop onto an excited electronic potential energy surface, remain there for several vibrational periods, and then return to the ground electronic surface. This process takes place in parallel with the normal reaction confined to the ground-state surface. Thus, the flux partially bifurcates so that part traverses a path on the ground-state surface and part traverses a path on an excited-state surface before returning to the lowest surface. In very energetic systems, such as those arising from photodissocia-

tion, chemiluminescence, or electronically excited reagents, electronic surfaces are closely spaced and products are often produced in different electronic states (2). In contrast, reactions starting and ending on the ground electronic state are normally presumed to occur on only that one potential energy surface. However, we believe that the results of the present experiments provide evidence of a reaction in which this is not the case.

The system under investigation is the bimolecular chemical reaction  $K + NaBr \rightarrow KBr + Na$ . This reaction has negligible activation energy; the reagents approach each other to within bonding distance and react on nearly every collision. In our experiments, which are carried out with crossed molecular beams of NaBr and K, the reaction is not artificially restricted, as it would be if the reaction were initially bound in a van der Waals complex. The reaction process is thus representative of normally occurring processes that include the entire array of thermal collision energies, impact parameters, and orientations. The reaction is probed spectroscopically by placing the molecular beam crossing region inside the cavity of a continuous-wave dye laser that is tuned to wavelengths not absorbed by either reagents or products. The transient species undergoing reaction, denoted as  $[K \cdot Br \cdot Na]$ , absorb laser light, producing excited  $[K \cdot Br \cdot Na]^*$ . These excited species can decompose reactively to give KBr and  $Na^*$ . The "laser-assisted" reaction is thus monitored by the *D* line emission from the  $Na^*$  atomic levels  $^2P_{1/2}$  and  $^2P_{3/2}$ , at 589.6 and 589.0 nm, respectively. This emission is passed through an interference filter and monitored by a photomultiplier as the excitation wavelength is varied. Typical laser-assisted signals from  $Na^*$  are  $\approx 200 \text{ s}^{-1}$ , in rough agreement with estimates (3) that are based on the assumption of molecular beam densities, zero activation energy for the dark reaction, a collision lifetime of  $\approx 3 \text{ ps}$ , and a circulating intracavity power of  $\approx 200 \text{ W}$ . The signal size is thus consistent with the excitation of a minute fraction (3) of the transient reacting species ( $\approx 5 \times 10^{-6}$ ), and the highly rarified molecular beam conditions minimize other interferences.

Previous measurements (4) were made with the use of an interference filter that passed only the sodium *D*<sub>2</sub> line at 589.0 nm, which corresponds to the transition  $^2P_{3/2} \rightarrow ^2S_{1/2}$ . Because different molecular electronic states of the reaction intermediate or transition region species correlate with different atomic fine structure states of the product, we also investigated the emission from the *D*<sub>1</sub> line at 589.6 nm ( $^2P_{1/2} \rightarrow ^2S_{1/2}$ ) using a different interference filter. The measured excitation spectra are differ-

Chemistry Department and Rice Quantum Institute, Rice University, Houston, TX 77251.

\*Present address: Analytical Chemistry Division, Oak Ridge National Laboratory, Oak Ridge, TN 37831-6142.

†To whom correspondence should be addressed.